Heat transfer measurements in rotating-disc systems Part 1: The free disc

A. Northrop* and J. M. Owen
Thermo-Fluid Mechanics Research Centre, School of Engineering & Applied Sciences, University of Sussex, Sussex, UK

Received 28 February 1987; accepted 11 June 1987

Heat transfer measurements have been made with an internally heated disc of 950 mm diameter rotating at speeds up to 3000 r/min in air. Tests were conducted for four different radial temperature profiles: in three, the temperature increased with radius; in the fourth, it decreased. Local and average Nusselt numbers were determined from the numerical solutions of Laplace's equation (using the measured heat input and surface temperatures as boundary conditions) and from fluxmeters embedded in the surface of the disc. Over most of the disc surface, and for most of the tests, these experimentally measured Nusselt numbers were in reasonable agreement with values obtained from existing solutions of the energy integral equation for turbulent flow over a free disc. Having validated the experimental technique on the free disc, we use it in Part 2 to study the heat transfer inside a rotating cavity.

Keywords: heat transfer; rotating disc; free disc

Introduction

A rotating disc provides an idealized model with which to study the flow and heat transfer that occur inside the rotors of turbomachinery (see Ref. 1). As shown in Figure 1, the gas turbine provides many examples of rotating-disc systems: a turbine disc rotating close to a stationary casing (the "rotor-stator system") or two corotating compressor discs sealed at their periphery (the "rotating cavity") are just two such cases. However, the most fundamental rotating-disc system is the "free disc": a disc rotating in an otherwise quiescent environment. Aspects of free-disc flow appear in other rotating-disc systems, and a large amount of theoretical and experimental work has been devoted to the fluid dynamics and heat transfer of such flows. Since there are reasonable experimental correlations and theoretical results for heat transfer from the free disc, it provides a useful datum with which to compare new experimental data and to judge new experimental techniques.

Part 1 of this two-part paper is concerned solely with heat transfer from the free disc. The relevant literature is reviewed in the second section, the experimental apparatus and data analysis are described in the third and fourth sections, and in the last section the heat transfer measurements are compared with theoretical values. In Part 2 (referred to below as II), the same heat transfer techniques are applied to a rotating cavity with a radial outflow of coolant.

Heat transfer from the free disc

For the free disc, Dorfman[2] obtained solutions of the laminar and turbulent energy integral equations, from which the local Nusselt number, Nu, is given in the form

$$\mathrm{Nu}=\frac{\mathrm{Pr}}{\Delta T}\frac{\mathrm{d}}{\mathrm{d}r}(r(\Delta T)R_{\mathrm{T}}) \tag{1}$$

where

$$R_{\mathrm{T}}^{m+2}=(m+1)A_{\mathrm{T}}^{-1}r^{-(m+3)}\Delta T^{-(m+1)}\mathrm{Re}_{\phi}^{*}\int_{0}^{r}r^{m+2}\Delta T^{m+1}\,\mathrm{d}r \tag{2}$$

and for turbulent flow $m=1$ and $A_{\mathrm{T}}\simeq 136\,\mathrm{Pr}^{0.5}$. The average Nusselt number is

$$\mathrm{Nu}_{\mathrm{av}}=4\mathrm{Pr}R_{\mathrm{R}} \tag{3}$$

where R_{T} is evaluated at $r=b$.

For the special case of the "power-law profile" of the form

$$\Delta T=cr^{n} \tag{4}$$

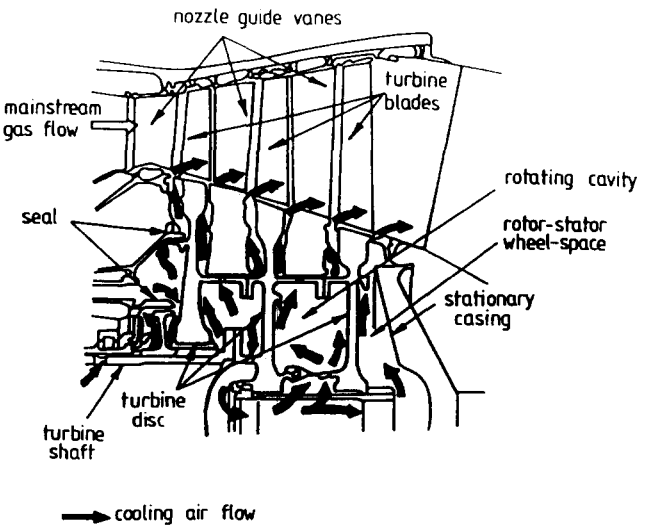

Figure 1 An air-cooled gas turbine rotor

* Presently at H&N Computing Services, Eastbourne, Sussex, UK

where c and n are constants, Equations 1 and 3 reduce to

$$Nu = 0.0197(n+2.6)^{0.2} Pr^{0.6} Re_\phi^{*0.8} \quad (5)$$

and

$$Nu_{av} = 0.0197(n+2)(n+2.6)^{-0.8} Pr^{0.6} Re_\phi^{0.8} \quad (6)$$

For air (Pr = 0.72) and for an isothermal disc ($n = 0$) these equations simplify to

$$Nu = 0.0196 Re_\phi^{*0.8} \quad (7)$$

and

$$Nu_{av} = 0.0151 Re_\phi^{0.8} \quad (8)$$

which agree, for $Re_\phi^* > 2.4 \times 10^5$, with the data of Cobb and Saunders[3] and Dennis, Newstead, and Ede.[4] McComas and Hartnett[5] obtained a value of 0.0138 rather than 0.0151 for the constant of proportionality in their correlations for the average Nusselt number.

For air with a quadratic temperature rise ($n = 2$) on the disc, Equation 6 becomes

$$Nu_{av} = 0.0191 Re_\phi^{0.8} \quad (9)$$

which gives values slightly lower than the correlation obtained by Owen, Haynes, and Bayley[6] for $2 \times 10^5 < Re_\phi < 4 \times 10^6$:

$$Nu_{av} = 0.0171 Re_\phi^{0.814} \quad (10)$$

It would appear therefore that, though not exact, Equation 1 can provide a reasonable estimate of heat transfer from the free disc.

For high values of Re_ϕ^*, where frictional heating can be significant, it is necessary to use the adiabatic disc temperature, $T_{s,ad}$, rather than the surface temperature, T_s, in the definition of ΔT. It was suggested by Owen[7] that

$$T_{s,ad} = T_\infty + \frac{\frac{1}{2}R\Omega^2 r^2}{C_p} \quad (11)$$

where T_∞ is the temperature of the fluid outside the boundary layer and, for moderate values of Pr, the recovery factor can be approximated by $R \simeq Pr^{1/3}$, such that

$$\Delta T = T - T_{s,ad} \quad (12)$$

Experimental apparatus

The rotating-disc rig

The rig was designed for rotating-cavity tests in which two corotating discs and a rotating peripheral shroud formed the cavity and through which cooling air could be blown axially or radially. However, the rig could be readily converted to a rotor-stator configuration, in which one disc was stationary, or to a free disc, in which one disc and the shroud were removed. It is the latter configuration that is described below; the rotating-cavity rig is described in II.

The rotating disc was of composite construction, details of which are given below, and was designed for rotation at speeds up to 5000 r/min. The overall thickness of the disc was 35 mm, and the inner and outer diameters were 152 and 950 mm. The disc was attached to one end of a hollow, horizontal, stainless-steel shaft which was 800 mm long and had inner and outer diameters of 88.6 and 101.3 mm. The shaft was mounted in two oil-lubricated ball-bearing assemblies fitted into steel housings and bolted to a cast-iron baseplate. The shaft was driven via pulleys, and toothed belts by a 90 kW thyristor-controlled dc motor, the speed of which could be controlled and measured to an accuracy of 1 r/min. A six-channel power slip-ring unit (with each ring capable of transmitting 20 A and 240 V) was mounted on the shaft between the bearings. A 60-channel instrumentation slip-ring unit (with silver rings and silver/graphite brushes for thermocouple signals) was fitted on a separate shaft attached to one end of the main hollow shaft; the disc was mounted on the other end.

The composite disc

Despite the problems associated with electrical connections being exposed to accelerations of order 10^4 g, it was considered that built-in heaters would provide better control of the power and temperature distribution than that attainable from stationary radiant heaters. Two types of heaters were tested: the first type used insulated constantan wire inside a spirally grooved steel shim bonded to the disc; the second type used a glass-fiber "heater mat" (manufactured and fitted by Lucas Aerospace). The first type of heater was prone to faults and

Notation

a_1, a_2	Constants
A_T	Nondimensional parameter in boundary layer energy equation
b	Outer radius of disc
c	Constant
C_p	Specific heat at constant pressure
k	Thermal conductivity
m	Constant
n	Constant
$Nu = qr/k\Delta T$	Local Nusselt number
$Nu_{av} = q_{av} b/k\Delta T_{av}$	Average Nusselt number
Pr	Prandtl number
q	Heat flux
q_G	Heat flux generated at interface
r	Radial coordinate
r_i	Inner radius of disc
R	Recovery factor
$Re_\phi^* = \Omega r^2/\nu$	Local rotational Reynolds number
$Re_\phi = \Omega b^2/\nu$	Disc rotational Reynolds number
R_T	Nondimensional parameter in energy integral equation
T	Temperature
V	Voltage
$x = r/b$	Nondimensional radial coordinate
z	Axial coordinate
ΔT	Temperature difference between disc surface and surrounding fluid
κ	Thermal conductivity
ν	Kinematic viscosity
τ	Temperature
Ω	Angular speed of disc
Subscripts	
ad	Adiabatic value
av	Radially weighted average value
0	Reference value
s	Surface of disc
∞	Free-stream value

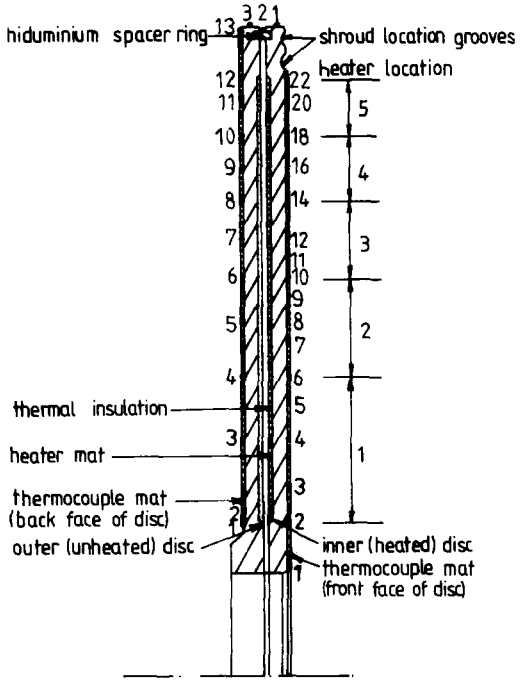

Figure 2 Details of the composite disc. Thermocouple locations are shown by 1, 2, 3, etc.; fluxmeters are fitted on the front face at 4, 8, 12, 16, and 20

failed to produce axisymmetrix heating; the second, which was successful, is described below.

Referring to Figure 2, note that the composite disc was made from two steel discs ($k = 48$ W/m K) of thickness 9.5 mm separated by a 13-mm thickness of Rohacell foam insulation ($k = 0.05$ W/m K). The heater mat was laminated from eight annular layers of glass-fiber-reinforced epoxy resin ($k = 0.27$ W/m K) with plasma-sprayed-metal resistance-heating elements sandwiched in the middle. The resulting mat, which had inner and outer radii of 112 mm and 441 mm and an overall thickness of 1 mm, was bonded to the internal face of the inner steel disc. Inside the mat were five separate annular heaters, each with approximately the same area and resistance of 12 Ω.

When bonded to the discs, the heater mat was capable of producing up to 24 kW of power, and it could withstand temperatures up to 150°C continuously and accelerations up to 15,000 g. Current to the five heater circuits was supplied through the power slip-rings via radial conductors located inside the Rohacell insulation. The power to each heater, which was regulated by a thyristor controller, was measured by a calibrated electrodynamic wattmeter with an accuracy of 1% f.s.d. (on the 5-kW range, the maximum error was 50 W).

A "thermocouple mat" was bonded to each of the external faces of the composite disc. These mats were similar to the heater mat but were only 0.8 mm thick and did not contain heating elements. One reason for their use was that thermocouples and fluxmeters could be embedded in the disc surface without slotting the highly stressed steel discs. Another reason was that the temperature disturbance error can be reduced by matching the thermal conductivity of the adhesive bonding the thermocouples to that of the substrate. (The effects of such disturbance errors on the calculation of Nusselt numbers are discussed in Refs. 8 and 9.)

Referring to Figure 2, note the following points. A peripheral spacer ring was fitted into grooves on the internal face of the two steel discs. From stress considerations, the ring was made from a lightweight aluminum alloy ("hiduminium" with a conductivity of $k = 184$ W/m K). The ring and the peripheral bolts used to clamp the discs together provided a thermal path between the two discs: this is discussed in greater detail in the next section. In addition, two circular grooves (used to locate the shrouds in the rotating-cavity tests) on the external face of the heated steel disc reduced the effective outer diameter for the free-disc tests to 443 mm. For these tests, the central hole was sealed with a glass-fiber mat bonded to the disc so as to be flush with the thermocouple mat on the front face of the disc.

Instrumentation

A total of 23 thermocouples was embedded in the thermocouple mat on the front face and 13 in the back face of the disc. In addition, three thermocouples were attached to the periphery of the disc, and five were embedded in the heater mat. The copper-constantan thermocouples were made from enameled wires of 0.15 mm diameter which were cemented into grooves in the mat using Araldite epoxy resin.

Five fluxmeters, manufactured by RDF Corporation, were embedded at the radially weighted midpoints of the heaters in the thermocouple mat on the front face. Each fluxmeter was made from a thin foil thermopile encapsulated in polyimide film. The approximate size was 17 mm × 6 mm × 0.3 mm, and the nominal output was 0.4 μV m^2 W^{-1}. The fluxmeters were fitted with the longer side in the tangential direction on the disc: for axisymmetric heating, this minimized errors due to spatial variation of heat flux.

The wires from the thermocouples and fluxmeters were brought out to a "connecting" ring, fitted with Klippon terminal blocks, which was attached to the back of the disc. The thermocouple leads were joined to copper wires at this point, and the temperature of the terminal blocks (used as the "cold-junction" reference) was measured by a semiconductor temperature sensor (adjusted to give an output of 100 mV K^{-1}) fixed to the ring. The signals from the sensor, thermocouples, and fluxmeters were taken out through the instrumentation slip rings and were measured by a Solartron data logger with an accuracy of 1 μV (which corresponds to approximately 0.03°C for copper-constantan thermocouples).

Data analysis

Only the salient features of the data analysis are presented below; the reader is referred to Northrop[10] for more details.

Data acquisition

The Solartron data logger was interfaced to a PDP11/34 minicomputer, and the raw data from the thermocouples, temperature sensors, and fluxmeters were stored on magnetic disc for subsequent analysis. Typically, 100 sets of readings were made at a rate of 33 readings per second, and ensemble averages were used to calculate the temperatures for each thermocouple. The 95% confidence intervals of the temperatures were usually within 0.2°C of the average readings; data that were more than three standard deviations from the average were rejected.

The averaged surface temperatures on the disc were fitted radially using VSMOOTH, a cubic-spline-smoothing subroutine that used statistical techniques to optimize the location and number of "knots" (see Ref. 11). The smoothed temperatures and the measured heater powers were then used as boundary conditions for the solution of Laplace's equation, as discussed below.

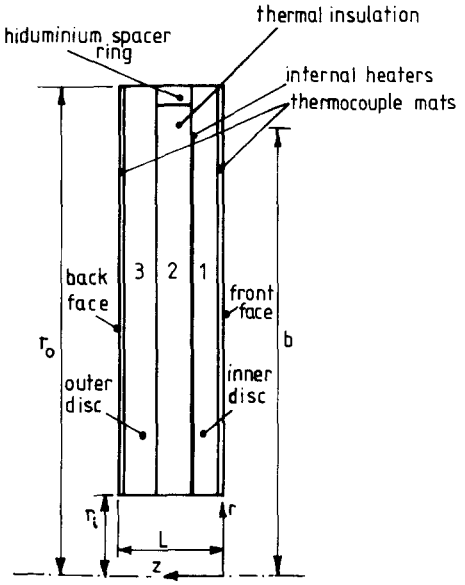

Figure 3 Composite-disc model used for the conduction solution

Solution of Laplace's equation

The solution of Laplace's equation has been used to obtain estimates of the average heat flux from a radiantly heated rotating disc (see Refs. 6, 12, and 13). Accurate local fluxes are difficult to achieve unless the local heat input can be determined precisely. This is difficult with radiant heating, but is easier with the built-in electrical heaters used in the current experiments. If the rotating disc could be perfectly insulated on its back face and periphery, then the local heat flux could be determined directly from the measured internal heater power. Since perfect insulation is impossible to achieve, it is necessary to solve Laplace's equation to determine the local flux.

For axisymmetric heating, Laplace's equation can be written in cylindrical polar coordinates as

$$\frac{\partial^2 T}{\partial r^2}+\frac{1}{r}\frac{\partial T}{\partial r}+\frac{\partial^2 T}{\partial z^2}=0 \tag{13}$$

Figure 3 shows the simplified representation of the composite disc that was used in the present analysis. Laplace's equation was separately applied to the two steel discs (sections labeled 1 and 3) and to the Rohacell insulation (section 2). The heater mat was modeled as a plane heat source on the boundary of sections 1 and 2, and allowance was made for the thermocouple mats on the external faces of sections 1 and 3. Details of the boundary conditions are given below.

Boundary conditions at the interfaces between the sections. The continuity of heat flux flowing axially across the interface at $z=z_0$, say, between the two materials of respective conductivities k and κ and temperatures T and τ, implies that

$$k\left(\frac{\partial T}{\partial z}\right)_{z_0}-\kappa\left(\frac{\partial \tau}{\partial z}\right)_{z_0}=q_G \tag{14}$$

where q_G is the heat flux generated at the interface. For the interface between sections 1 and 2, q_G is determined by dividing the measured power input to a heater by the area of that heater; for all other interfaces, q_G is zero. Continuity of temperature at all interfaces (assuming no contact resistance) necessitates that

$$T=\tau \qquad \text{at } z=z_0 \tag{15}$$

Boundary conditions on the front and back faces: $z=0$ and $z=L$. For these faces, the smoothed surface temperatures were used as boundary conditions.

Boundary conditions for the inner and outer radii: $r=r_i$ and $r=r_0$. For the inner radius, the one-dimensional assumption (used in Refs. 12 and 13) was used, such that

$$\left(\frac{\partial^2 T}{\partial z^2}\right)_{r_i}=\left[\frac{1}{r}\frac{\partial}{\partial r}\left(\frac{\partial T}{\partial r}\right)\right]_{r_i}=0 \tag{16}$$

Since the periphery of the disc was insulated with Rohacell, the adiabatic condition was used at $r=r_0$, where

$$\left(\frac{\partial T}{\partial r}\right)_{r_0}=0 \tag{17}$$

The spacer ring. The high conductivity ($k=184$ W/m K) of the hiduminium spacer ring created a thermal path between the two steel discs. Since the contact resistance between the ring and the discs was unknown, an empirical "effective conductivity" was used. From numerical "experiments," a value of 6 W/m K was chosen: this value, which was in the range 5 to 22 W/m K obtained from the data of Lewis and Perkins,[14] produced results consistent with Dorfman's theory (Equation 1). For $r/b<0.8$, a variation in the effective conductivity from 5 to 22 would typically alter the computed local Nusselt numbers by less than 5%; for $r/b>0.8$ (and for the radially weighted average Nusselt numbers), the effect is likely to be greater.

Computation of heat flux

Using the boundary conditions stated above, Laplace's equation was solved numerically. A total of 9 axial and 17 radial grid points was used, and Equation 13 and the boundary conditions were discretized using second-order Taylor-series approximations. The resulting system of equations was solved by Gaussian elimination to produce temperatures at the internal nodes.

The local surface heat fluxes were computed from a second-order difference formula, and the local Nusselt numbers were calculated from the definitions given in the notation list. The radially weighted average heat flux was computed from the local values by Simpson's rule. As a check on the numerical accuracy, the computed total heat flow rate from the external surfaces of the disc was compared with the measured power input. For most tests, the error was less than 1%. This numerical heat balance cannot, however, be regarded as a physical balance.

No allowance was made for radiation from the disc surface to the surroundings. Although radiation had only a relatively small effect when convective heat transfer was high (at large Reynolds numbers), it could be significant at the smaller values of Re_ϕ. Estimates of radially weighted blackbody radiation (the emissivity of the thermocouple mat was nearly unity) from the disc suggests that the absolute difference between the value of Nu_{av} obtained from the conduction solution and the true value should be less than 150.

Heat transfer measurements

Radial temperature distribution

Varying the power input to each of the five heaters made it possible to produce different radial temperature distributions on the front face of the disc. Examples of four of these distributions, for $Re_\phi \simeq 10^6$, are shown in Figure 4. The temperature difference

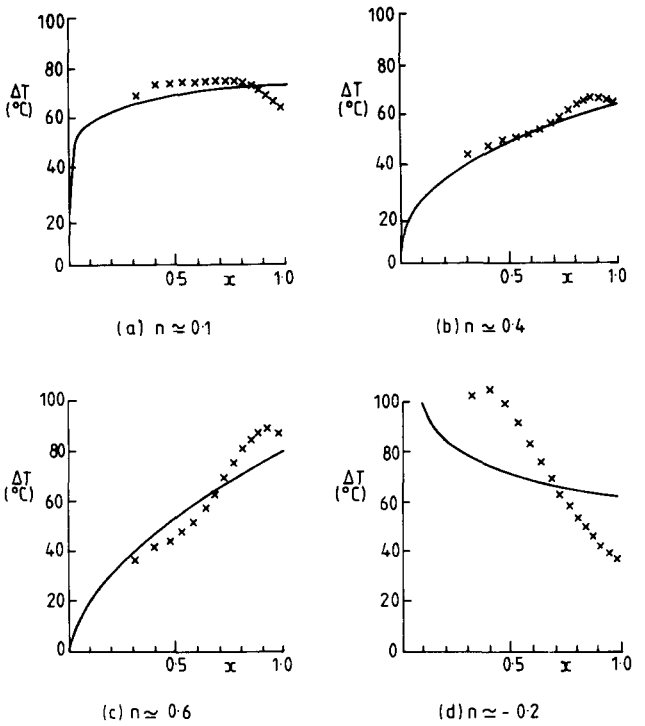

Figure 4 Examples of the four temperature profiles tested: ×, experimental data; ——, Equation 4

ΔT can be approximated by a power law of the form given in Equation 4 with values of n (obtained from least-squares fits) of 0.1, 0.4, 0.6, and −0.2. Although they do not give an accurate representation of the measured temperature, the power-law profiles do provide a convenient way of distinguishing the four different temperature distributions.

Local Nusselt numbers

The conduction solution. Figures 5 to 8 show the radial variation of the local Nusselt numbers for each of the four temperature distributions referred to above. The measured values were obtained using the conduction solution described in the previous section; the theoretical curves were calculated from Equation 1. The turning point in the measured Nusselt numbers at $x \simeq 0.9$ is caused by the assumed conditions at the disc tip (see the subsection on the solution of Laplace's equation), and measured values for $x > 0.9$ should be disregarded.

Figure 5 shows the results for a temperature distribution approximated by the form $T \propto r^{0.1}$ (that is, $n = 0.1$ in Equation 4). For $0.4 < x < 0.9$, the measured Nusselt numbers are in good agreement with the theoretical curves for $0.28 \leqslant \mathrm{Re}_\phi/10^6 \leqslant 3.2$. At lower values of Re_ϕ and smaller values of x, where the Nusselt numbers are relatively small, the effects of radiation and free convection can be significant. These effects were estimated for the results at $\mathrm{Re}_\phi = 5 \times 10^4$, where the calculated radiation losses accounted for approximately half the measured heat flux; allowing for both radiation and free convection, the difference between the maximum measured Nusselt number and the theoretical value was reduced from over 200 to approximately 50. Considering all the effects referred to above, the agreement between the measured and the theoretical local Nusselt numbers is considered to be acceptable.

The tests for $n \simeq 0.4$, 0.6, and −0.2, the results of which are shown in Figures 6, 7, and 8, respectively, were conducted over a smaller range of Reynolds numbers than those in Figure 5. Again, bearing in mind the above comments about the effects of radiation, free convection and boundary conditions, the agreement between the measured values and Equation 1 is reasonable.

Fluxmeter measurements. The fluxmeters had nonlinear characteristics, and *in situ* calibration was carried out to

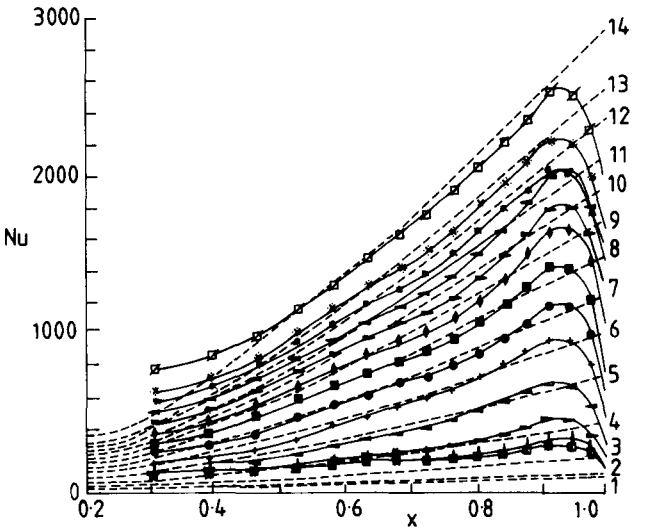

Figure 5 The radial variation of local Nusselt numbers, obtained from the conduction solution, for $n \simeq 0.1$; ——, conduction solution; – – –, Equation 1

$\mathrm{Re}_\phi/10^6$	0.05	0.07	0.14	0.28	0.55	0.82	1.1
Conduction solution	×	□	◊	▻	◅	+	●
Equation 1	1	2	3	4	5	6	7
$\mathrm{Re}_\phi/10^6$	1.4	1.6	1.9	2.1	2.4	2.7	3.2
Conduction solution	■	♦	▻	◅	✱	✳	⊠
Equation 1	8	9	10	11	12	13	14

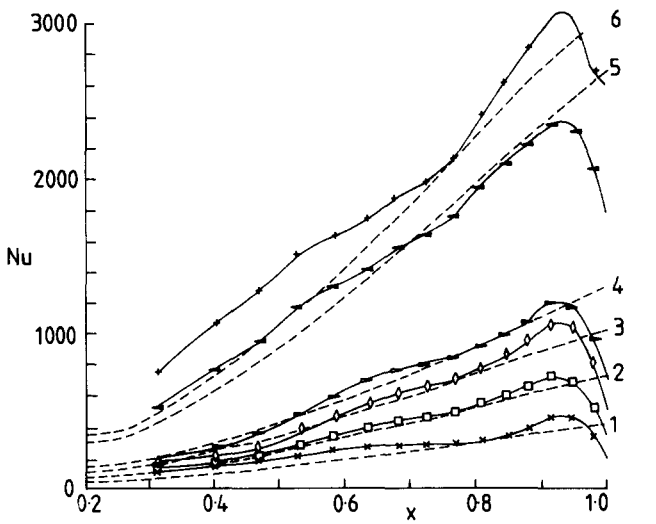

Figure 6 The radial variation of local Nusselt numbers, obtained from the conduction solution, for $n \simeq 0.4$: ——, conduction solution; – – –, Equation 1

$\mathrm{Re}_\phi/10^6$	0.28	0.55	0.83	1.1	2.7	3.1
Conduction solution	×	□	◊	▻	◅	+
Equation 1	1	2	3	4	5	6

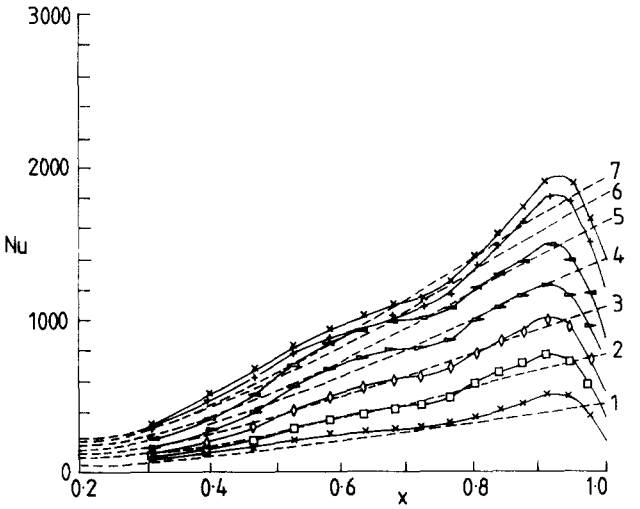

Figure 7 The radial variation of local Nusselt numbers, obtained from the conduction solutions, for $n \simeq 0.6$: ——, conduction solution; – – –, Equation 1

$Re_\phi/10^6$	0.28	0.55	0.83	1.1	1.4	1.6	1.7
Conduction solution	×	□	◊	▷	◁	+	✳
Equation 1	1	2	3	4	5	6	7

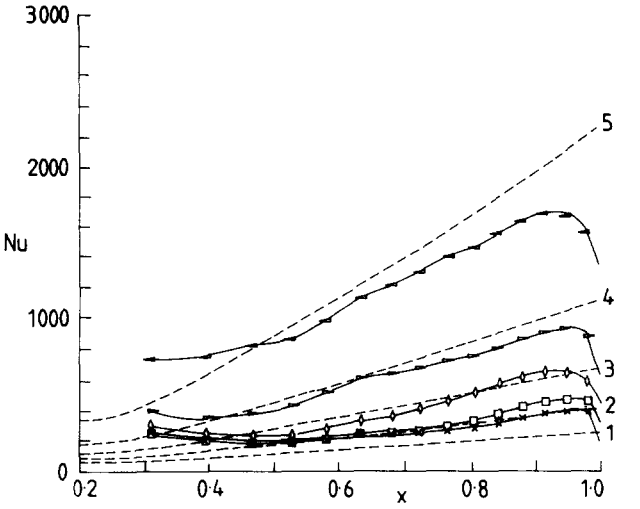

Figure 8 The radial variation of local Nusselt numbers, obtained from the conduction solution, for $n \simeq -0.2$: ——, conduction solution; – – –, Equation 1

$Re_\phi/10^6$	0.14	0.27	0.55	1.1	2.7
Conduction solution	×	□	◊	▷	◁
Equation 1	1	2	3	4	5

determine the relationship between the output voltage V and the heat flux q. It was assumed that $q = a_1 V + a_2 V^2$, where a_1 and a_2 are temperature-dependent constants. For each fluxmeter, the values of a_1 and a_2 were chosen from a least-squares fit to the values of flux obtained from the conduction solution; further details are given in Ref. 10. Although not completely independent, the fluxmeter results presented below provide an alternative picture to that obtained from the conduction solution.

Figures 9 to 12 show the comparison between the local Nusselt numbers determined from the calibrated fluxmeters and the theoretical results calculated from Equation 1. Comparing Figure 9 with Figure 5 shows, not surprisingly, that the fluxmeter results agree with the theoretical curves over similar ranges of x and Re_ϕ. However, unlike the conduction solution, the fluxmeters do not suggest that there is a turning point at $x \simeq 0.9$, although there are insufficient experimental points to confirm this. The agreement between the fluxmeters and the theoretical curves is also reasonable for the other temperature profiles, as can be seen in Figures 10 to 12.

Average Nusselt numbers

Figure 13 shows the variation in the average Nusselt number with rotational Reynolds number for each of the four different

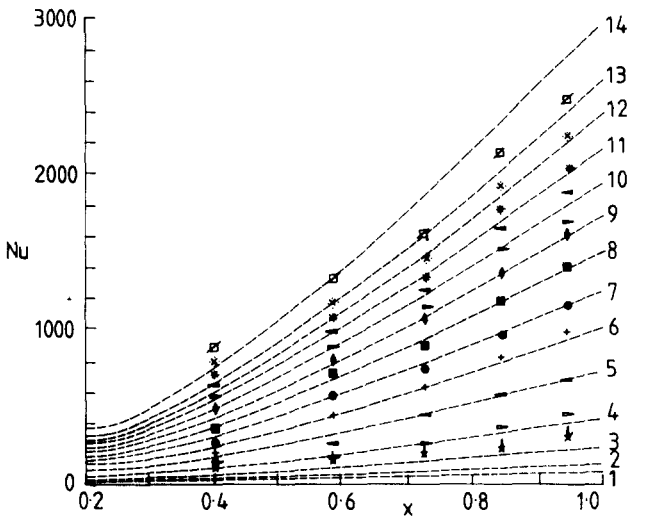

Figure 9 The radial variation of local Nusselt numbers, obtained from the calibrated fluxmeters, for $n \simeq 0.1$: – – –, Equation 1

$Re_\phi/10^6$	0.049	0.070	0.14	0.28	0.55	0.82	1.1
Fluxmeter	×	□	◊	▻	◅	+	●
Equation 1	1	2	3	4	5	6	7
$Re_\phi/10^6$	1.4	1.6	1.9	2.1	2.4	2.7	3.2
Fluxmeter	■	♦	▬	▬	✱	✳	⊠
Equation 1	8	9	10	11	12	13	14

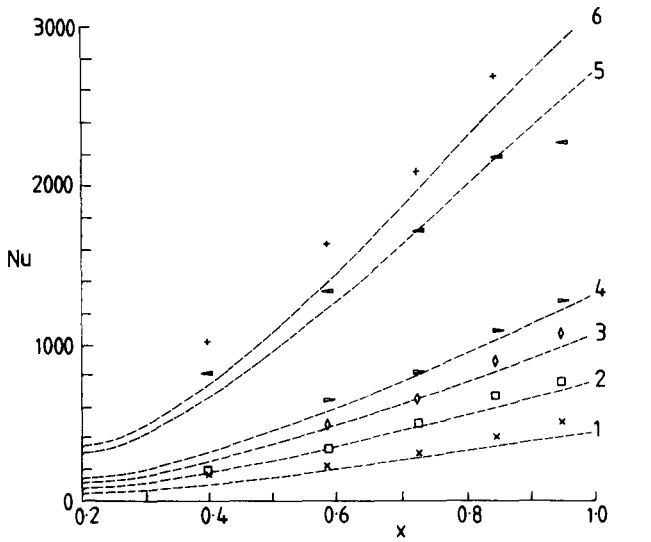

Figure 10 The radial variation of local Nusselt numbers, obtained from the calibrated fluxmeters, for $n \simeq 0.4$: – – –, Equation 1

$Re_\phi/10^6$	0.28	0.55	0.83	1.1	2.7	3.1
Fluxmeter	×	□	◊	▻	◅	+
Equation 1	1	2	3	4	5	6

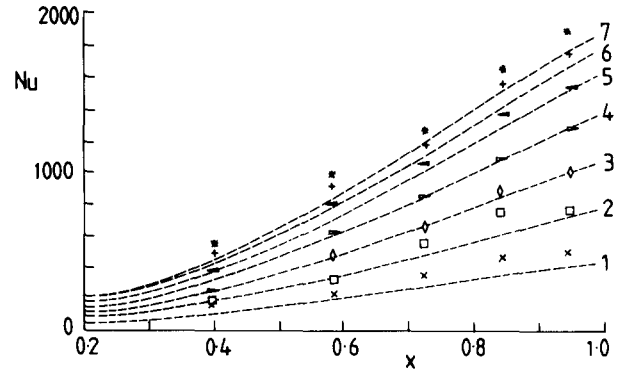

Figure 11 The radial variation of local Nusselt numbers, obtained from the calibrated fluxmeters, for $n \simeq 0.6$: ---, Equation 1

$Re_\phi/10^6$	0.28	0.55	0.83	1.1	1.4	1.6	1.7
Fluxmeter	×	□	◊	▷	◁	+	*
Equation 1	1	2	3	4	5	6	7

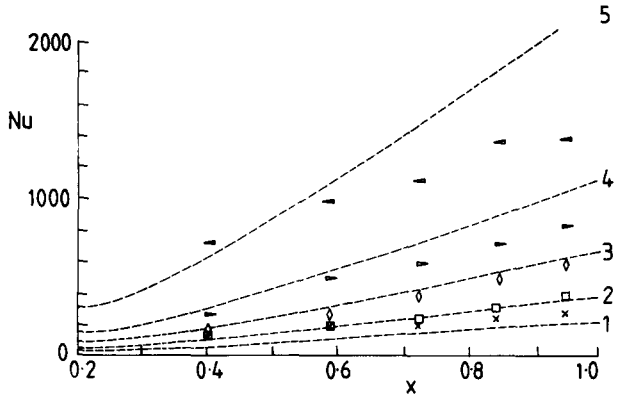

Figure 12 The radial variation of local Nusselt numbers, obtained from the calibrated fluxmeters, for $n \simeq -0.2$: ---, Equation 1

$Re_\phi/10^6$	0.14	0.27	0.55	1.1	2.7
Fluxmeter	×	□	◊	▷	◁
Equation 1	1	2	3	4	5

temperature distributions. Owing to the inaccuracies in the measured fluxes at low values of the Nusselt number, only the results for turbulent flow are shown. The experimental values were obtained from the integrated conduction solution, and the theoretical curves were calculated from Equation 3.

The experimental results were not corrected for radiation, but the agreement between the experimental and theoretical values is, in the main, good. Since the error in the conduction solution for $x > 0.9$ reduces the experimental average Nusselt number and radiation increases it, it would appear that these two effects are approximately self-canceling.

Conclusions

Free-disc heat transfer tests have been conducted with a disc of 950 mm diameter rotating at speeds up to 3000 r/min in air. By means of five electric heaters embedded inside the disc, its radial temperature distribution could be altered. Tests were carried out for four different distributions: the temperature increased with radius in three of the distributions and decreased in the fourth. The heat fluxes were obtained from the numerical solution of Laplace's conduction equation (using the measured surface temperatures and electrical power input as boundary

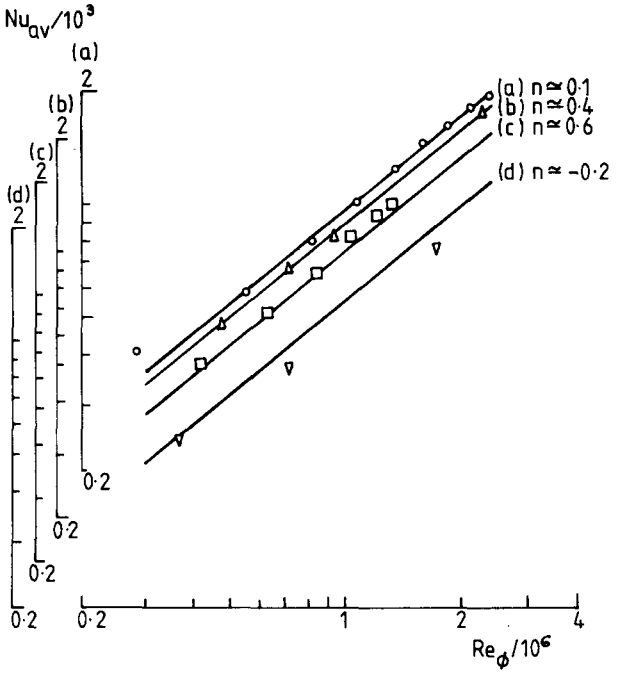

Figure 13 The variation of average Nusselt number with rotational Reynolds number for four different temperature profiles: ——, Equation 3

conditions) and from fluxmeters mounted in one of the surfaces of the disc. Apart from near the center (where radiation and free convection effects were significant) and near the outer part of the disc (where the conduction solution was inaccurate), the measured local and average Nusselt numbers were in reasonable agreement with Dorfman's[2] solution of the turbulent energy integral equation over a wide range of rotational Reynolds numbers.

Having validated the experimental technique on a reasonably well-understood test case, we use it in II to measure the Nusselt numbers in a rotating cavity with a radial outflow of cooling air.

References

1 Owen, J. M. Fluid flow and heat transfer in rotating disc systems. In: *Heat and Mass Transfer in Rotating Machinery*, eds. Metzger, D. E. and Afgan, N. H., Hemisphere, Washington, 1984

2 Dorfman, L. A. Hydrodynamic resistance and the heat loss of rotating solids. Oliver and Boyd, Edinburgh, 1963

3 Cobb, E. C. and Saunders, O. A. Heat transfer from a rotating disk. *Proc. R. Soc. Lond.*, 1956, **A236**, 343

4 Dennis, R. W., Newstead, C., and Ede, A. J. Heat transfer from a rotating disc in cross-flow. Heat Transfer 1970, 4th Int. Heat Transfer Conf., Versailles, III, F.C.7.1

5 McComas, S. T. and Hartnett, J. P. Temperature profiles associated with a single disk rotating in still air. Heat Transfer 1970, 4th Int. Heat Transfer Conf., Versailles, III, F.C.7.7

6 Owen, J. M., Haynes, C. M., and Bayley, F. J. Heat transfer from an air-cooled rotating disc. *Proc. R. Soc. Lond.*, 1974, **A336**, 453

7 Owen, J. M. The Reynolds analogy applied to flow between a rotating and stationary disc. *Int. J. Heat Mass Transfer*, 1971, **14**, 451

8 Owen, J. M. On the computation of heat transfer coefficients from imperfect temperature measurements. *J. Mech. Engng Sci.*, 1979, **21**, 323

9 Long, C. A. The effects of thermocouple disturbance errors on local heat transfer coefficients. Test and Transducer Conference, Wembley, London, 1985, **3**, 73

10 Northrop, A. Heat transfer in a cylindrical rotating cavity. D.Phil. thesis, University of Sussex, England, 1984

11 Powell, M. J. D. Curve fitting by splines in one variable. In: *Numerical Approximations to Functions and Data*, ed. Haynes, J. G., Athlone Press, University of London, 1970

12 Owen, J. M. and Bilimoria, E. D. Heat transfer in rotating cylindrical cavities. *J. Mech. Engng Sci.*, 1977, **17**, 175

13 Owen, J. M. and Onur, H. S. Convective heat transfer in a rotating cylindrical cavity. *J. Engng Power*, 1983, **195**, 265

14 Lewis, D. V. and Perkins, H. C. Heat transfer at the interface of stainless steel and aluminium—the influence of surface conditions on the directional effect. *Int. J. Heat Mass Transfer*, 1968, **11**, 1371